3-1-1995

Jet production in high Q^2 deep-inelastic ep scattering at HERA

M. Derrick
Argonne National Laboratory

D. Krakauer
Argonne National Laboratory

S. Magill
Argonne National Laboratory

D. Mikunas
Argonne National Laboratory

B. Musgrave
Argonne National Laboratory

See next page for additional authors

Jet production in high Q^2 deep-inelastic ep scattering at HERA

ZEUS Collaboration

Abstract

Two-jet production in deep-inelastic electron-proton scattering has been studied for $160 < Q^2 < 1280$ GeV^2, $0.01 < x < 0.1$ and $0.04 < y < 0.95$ with the ZEUS detector at HERA. The kinematic properties of the jets and the jet production rates are presented. The partonic scaling variables of the two-jet system and the rate of two-jet production are compared to perturbative next-to-leading order QCD calculations.

The ZEUS Collaboration

M. Derrick, D. Krakauer, S. Magill, D. Mikunas, B. Musgrave, J. Repond, R. Stanek, R.L. Talaga, H. Zhang
Argonne National Laboratory, Argonne, IL, USA [p]

R. Ayad[1], G. Bari, M. Basile, L. Bellagamba, D. Boscherini, A. Bruni, G. Bruni, P. Bruni, G. Cara Romeo, G. Castellini[2], M. Chiarini, L. Cifarelli[3], F. Cindolo, A. Contin, I. Gialas, P. Giusti, G. Iacobucci, G. Laurenti, G. Levi, A. Margotti, T. Massam, R. Nania, C. Nemoz, F. Palmonari, A. Polini, G. Sartorelli, R. Timellini, Y. Zamora Garcia[1], A. Zichichi
University and INFN Bologna, Bologna, Italy [f]

A. Bargende, J. Crittenden, K. Desch, B. Diekmann[4], T. Doeker, M. Eckert, L. Feld, A. Frey, M. Geerts, G. Geitz[5], M. Grothe, T. Haas, H. Hartmann, D. Haun[4], K. Heinloth, E. Hilger, H.-P. Jakob, U.F. Katz, S.M. Mari, A. Mass, S. Mengel, J. Mollen, E. Paul, Ch. Rembser, R. Schattevoy[6], D. Schramm, J. Stamm, R. Wedemeyer
Physikalisches Institut der Universität Bonn, Bonn, Federal Republic of Germany [c]

S. Campbell-Robson, A. Cassidy, N. Dyce, B. Foster, S. George, R. Gilmore, G.P. Heath, H.F. Heath, T.J. Llewellyn, C.J.S. Morgado, D.J.P. Norman, J.A. O'Mara, R.J. Tapper, S.S. Wilson, R. Yoshida
H.H. Wills Physics Laboratory, University of Bristol, Bristol, U.K. [o]

R.R. Rau
Brookhaven National Laboratory, Upton, L.I., USA [p]

M. Arneodo[7], L. Iannotti, M. Schioppa, G. Susinno
Calabria University, Physics Dept.and INFN, Cosenza, Italy [f]

A. Bernstein, A. Caldwell, J.A. Parsons, S. Ritz, F. Sciulli, P.B. Straub, L. Wai, S. Yang, Q. Zhu
Columbia University, Nevis Labs., Irvington on Hudson, N.Y., USA [q]

P. Borzemski, J. Chwastowski, A. Eskreys, K. Piotrzkowski, M. Zachara, L. Zawiejski
Inst. of Nuclear Physics, Cracow, Poland [j]

L. Adamczyk, B. Bednarek, K. Eskreys, K. Jeleń, D. Kisielewska, T. Kowalski, E. Rulikowska-Zarębska, L. Suszycki, J. Zając
Faculty of Physics and Nuclear Techniques, Academy of Mining and Metallurgy, Cracow, Poland [j]

A. Kotański, M. Przybycień
Jagellonian Univ., Dept. of Physics, Cracow, Poland [k]

L.A.T. Bauerdick, U. Behrens, H. Beier[8], J.K. Bienlein, C. Coldewey, O. Deppe, K. Desler, G. Drews, M. Flasiński[9], D.J. Gilkinson, C. Glasman, P. Göttlicher, J. Große-Knetter, B. Gutjahr, W. Hain, D. Hasell, H. Heßling, H. Hultschig, Y. Iga, P. Joos, M. Kasemann, R. Klanner, W. Koch, L. Köpke[10], U. Kötz, H. Kowalski, J. Labs, A. Ladage, B. Löhr, M. Löwe, D. Lüke, O. Mańczak, J.S.T. Ng, S. Nickel, D. Notz, K. Ohrenberg, M. Roco, M. Rohde, J. Roldán, U. Schneekloth, W. Schulz, F. Selonke, E. Stiliaris[11], B. Surrow, T. Voß, D. Westphal, G. Wolf, C. Youngman, J.F. Zhou
Deutsches Elektronen-Synchrotron DESY, Hamburg, Federal Republic of Germany

H.J. Grabosch, A. Kharchilava, A. Leich, M. Mattingly, A. Meyer, S. Schlenstedt
DESY-Zeuthen, Inst. für Hochenergiephysik, Zeuthen, Federal Republic of Germany

G. Barbagli, P. Pelfer
University and INFN, Florence, Italy [f]

G. Anzivino, G. Maccarrone, S. De Pasquale, L. Votano
INFN, Laboratori Nazionali di Frascati, Frascati, Italy [f]

A. Bamberger, S. Eisenhardt, A. Freidhof, S. Söldner-Rembold[12], J. Schroeder[13], T. Trefzger
Fakultät für Physik der Universität Freiburg i.Br., Freiburg i.Br., Federal Republic of Germany [c]

N.H. Brook, P.J. Bussey, A.T. Doyle[14], I. Fleck, V.A. Jamieson, D.H. Saxon, M.L. Utley, A.S. Wilson
Dept. of Physics and Astronomy, University of Glasgow, Glasgow, U.K. [o]

A. Dannemann, U. Holm, D. Horstmann, T. Neumann, R. Sinkus, K. Wick
Hamburg University, I. Institute of Exp. Physics, Hamburg, Federal Republic of Germany [c]

E. Badura[15], B.D. Burow[16], L. Hagge, E. Lohrmann, J. Mainusch, J. Milewski, M. Nakahata[17], N. Pavel, G. Poelz, W. Schott, F. Zetsche
Hamburg University, II. Institute of Exp. Physics, Hamburg, Federal Republic of Germany [c]

T.C. Bacon, I. Butterworth, E. Gallo, V.L. Harris, B.Y.H. Hung, K.R. Long, D.B. Miller, P.P.O. Morawitz, A. Prinias, J.K. Sedgbeer, A.F. Whitfield
Imperial College London, High Energy Nuclear Physics Group, London, U.K. [o]

U. Mallik, E. McCliment, M.Z. Wang, S.M. Wang, J.T. Wu, Y. Zhang
University of Iowa, Physics and Astronomy Dept., Iowa City, USA [p]

P. Cloth, D. Filges
Forschungszentrum Jülich, Institut für Kernphysik, Jülich, Federal Republic of Germany

S.H. An, S.M. Hong, S.W. Nam, S.K. Park, M.H. Suh, S.H. Yon
Korea University, Seoul, Korea [h]

R. Imlay, S. Kartik, H.-J. Kim, R.R. McNeil, W. Metcalf, V.K. Nadendla
Louisiana State University, Dept. of Physics and Astronomy, Baton Rouge, LA, USA [p]

F. Barreiro[18], G. Cases, R. Graciani, J.M. Hernández, L. Hervás[18], L. Labarga[18], J. del Peso, J. Puga, J. Terron, J.F. de Trocóniz
Univer. Autónoma Madrid, Depto de Física Teóríca, Madrid, Spain [n]

G.R. Smith
University of Manitoba, Dept. of Physics, Winnipeg, Manitoba, Canada [a]

F. Corriveau, D.S. Hanna, J. Hartmann, L.W. Hung, J.N. Lim, C.G. Matthews, P.M. Patel, L.E. Sinclair, D.G. Stairs, M. St.Laurent, R. Ullmann, G. Zacek
McGill University, Dept. of Physics, Montreal, Quebec, Canada [a, b]

V. Bashkirov, B.A. Dolgoshein, A. Stifutkin
Moscow Engineering Physics Institute, Mosocw, Russia [l]

G.L. Bashindzhagyan, P.F. Ermolov, L.K. Gladilin, Y.A. Golubkov, V.D. Kobrin, V.A. Kuzmin, A.S. Proskuryakov, A.A. Savin, L.M. Shcheglova, A.N. Solomin, N.P. Zotov
Moscow State University, Institute of Nuclear Pysics, Moscow, Russia [m]

M. Botje, F. Chlebana, A. Dake, J. Engelen, M. de Kamps, P. Kooijman, A. Kruse, H. Tiecke, W. Verkerke, M. Vreeswijk, L. Wiggers, E. de Wolf, R. van Woudenberg
NIKHEF and University of Amsterdam, Netherlands [i]

D. Acosta, B. Bylsma, L.S. Durkin, K. Honscheid, C. Li, T.Y. Ling, K.W. McLean[19], W.N. Murray, I.H. Park, T.A. Romanowski[20], R. Seidlein[21]
Ohio State University, Physics Department, Columbus, Ohio, USA [p]

D.S. Bailey, G.A. Blair[22], A. Byrne, R.J. Cashmore, A.M. Cooper-Sarkar, D. Daniels[23], R.C.E. Devenish, N. Harnew, M. Lancaster, P.E. Luffman[24], L. Lindemann, J.D. McFall, C. Nath, A. Quadt, H. Uijterwaal, R. Walczak, F.F. Wilson, T. Yip
Department of Physics, University of Oxford, Oxford, U.K. [o]

G. Abbiendi, A. Bertolin, R. Brugnera, R. Carlin, F. Dal Corso, M. De Giorgi, U. Dosselli, S. Limentani, M. Morandin, M. Posocco, L. Stanco, R. Stroili, C. Voci
Dipartimento di Fisica dell' Universita and INFN, Padova, Italy [f]

J. Bulmahn, J.M. Butterworth, R.G. Feild, B.Y. Oh, J.J. Whitmore[25]
Pennsylvania State University, Dept. of Physics, University Park, PA, USA [q]

G. D'Agostini, G. Marini, A. Nigro, E. Tassi
Dipartimento di Fisica, Univ. 'La Sapienza' and INFN, Rome, Italy [f]

J.C. Hart, N.A. McCubbin, K. Prytz, T.P. Shah, T.L. Short
Rutherford Appleton Laboratory, Chilton, Didcot, Oxon, U.K. [o]

E. Barberis, N. Cartiglia, T. Dubbs, C. Heusch, M. Van Hook, B. Hubbard, W. Lockman, J.T. Rahn, H.F.-W. Sadrozinski, A. Seiden
University of California, Santa Cruz, CA, USA [p]

J. Biltzinger, R.J. Seifert, A.H. Walenta, G. Zech
Fachbereich Physik der Universität-Gesamthochschule Siegen, Federal Republic of Germany [c]

H. Abramowicz, G. Briskin, S. Dagan[26], A. Levy[27]
School of Physics,Tel-Aviv University, Tel Aviv, Israel [e]

T. Hasegawa, M. Hazumi, T. Ishii, M. Kuze, S. Mine, Y. Nagasawa, M. Nakao, I. Suzuki, K. Tokushuku, S. Yamada, Y. Yamazaki
Institute for Nuclear Study, University of Tokyo, Tokyo, Japan [g]

M. Chiba, R. Hamatsu, T. Hirose, K. Homma, S. Kitamura, Y. Nakamitsu, K. Yamauchi
Tokyo Metropolitan University, Dept. of Physics, Tokyo, Japan [g]

R. Cirio, M. Costa, M.I. Ferrero, L. Lamberti, S. Maselli, C. Peroni, R. Sacchi, A. Solano, A. Staiano
Universita di Torino, Dipartimento di Fisica Sperimentale and INFN, Torino, Italy [f]

M. Dardo
II Faculty of Sciences, Torino University and INFN - Alessandria, Italy [f]

D.C. Bailey, D. Bandyopadhyay, F. Benard, M. Brkic, M.B. Crombie, D.M. Gingrich[28], G.F. Hartner, K.K. Joo, G.M. Levman, J.F. Martin, R.S. Orr, C.R. Sampson, R.J. Teuscher
University of Toronto, Dept. of Physics, Toronto, Ont., Canada [a]

C.D. Catterall, T.W. Jones, P.B. Kaziewicz, J.B. Lane, R.L. Saunders, J. Shulman
University College London, Physics and Astronomy Dept., London, U.K. [o]

K. Blankenship, J. Kochocki, B. Lu, L.W. Mo
Virginia Polytechnic Inst. and State University, Physics Dept., Blacksburg, VA, USA [q]

W. Bogusz, K. Charchuła, J. Ciborowski, J. Gajewski, G. Grzelak, M. Kasprzak, M. Krzyżanowski, K. Muchorowski, R.J. Nowak, J.M. Pawlak, T. Tymieniecka, A.K. Wróblewski, J.A. Zakrzewski, A.F. Żarnecki
Warsaw University, Institute of Experimental Physics, Warsaw, Poland [j]

M. Adamus
Institute for Nuclear Studies, Warsaw, Poland [j]

Y. Eisenberg[26], U. Karshon[26], D. Revel[26], D. Zer-Zion
Weizmann Institute, Nuclear Physics Dept., Rehovot, Israel [d]

I. Ali, W.F. Badgett, B. Behrens, S. Dasu, C. Fordham, C. Foudas, A. Goussiou, R.J. Loveless, D.D. Reeder, S. Silverstein, W.H. Smith, A. Vaiciulis, M. Wodarczyk
University of Wisconsin, Dept. of Physics, Madison, WI, USA [p]

T. Tsurugai
Meiji Gakuin University, Faculty of General Education, Yokohama, Japan

S. Bhadra, M.L. Cardy, C.-P. Fagerstroem, W.R. Frisken, K.M. Furutani, M. Khakzad, W.B. Schmidke
York University, Dept. of Physics, North York, Ont., Canada [a]

[1] supported by Worldlab, Lausanne, Switzerland
[2] also at IROE Florence, Italy
[3] now at Univ. of Salerno and INFN Napoli, Italy
[4] now a self-employed consultant
[5] on leave of absence
[6] now at MPI Berlin
[7] now also at University of Torino
[8] presently at Columbia Univ., supported by DAAD/HSPII-AUFE
[9] now at Inst. of Computer Science, Jagellonian Univ., Cracow
[10] now at Univ. of Mainz
[11] supported by the European Community
[12] now with OPAL Collaboration, Faculty of Physics at Univ. of Freiburg
[13] now at SAS-Institut GmbH, Heidelberg
[14] also supported by DESY
[15] now at GSI Darmstadt
[16] also supported by NSERC
[17] now at Institute for Cosmic Ray Research, University of Tokyo
[18] on leave of absence at DESY, supported by DGICYT
[19] now at Carleton University, Ottawa, Canada
[20] now at Department of Energy, Washington
[21] now at HEP Div., Argonne National Lab., Argonne, IL, USA
[22] now at RHBNC, Univ. of London, England
[23] Fulbright Scholar 1993-1994
[24] now at Cambridge Consultants, Cambridge, U.K.
[25] on leave and partially supported by DESY 1993-95
[26] supported by a MINERVA Fellowship
[27] partially supported by DESY
[28] now at Centre for Subatomic Research, Univ.of Alberta, Canada and TRIUMF, Vancouver, Canada

[a] supported by the Natural Sciences and Engineering Research Council of Canada (NSERC)
[b] supported by the FCAR of Quebec, Canada
[c] supported by the German Federal Ministry for Research and Technology (BMFT)
[d] supported by the MINERVA Gesellschaft für Forschung GmbH, and by the Israel Academy of Science
[e] supported by the German Israeli Foundation, and by the Israel Academy of Science
[f] supported by the Italian National Institute for Nuclear Physics (INFN)
[g] supported by the Japanese Ministry of Education, Science and Culture (the Monbusho) and its grants for Scientific Research
[h] supported by the Korean Ministry of Education and Korea Science and Engineering Foundation
[i] supported by the Netherlands Foundation for Research on Matter (FOM)
[j] supported by the Polish State Committee for Scientific Research (grant No. SPB/P3/202/93) and the Foundation for Polish- German Collaboration (proj. No. 506/92)
[k] supported by the Polish State Committee for Scientific Research (grant No. PB 861/2/91 and No. 2 2372 9102, grant No. PB 2 2376 9102 and No. PB 2 0092 9101)
[l] partially supported by the German Federal Ministry for Research and Technology (BMFT)
[m] supported by the German Federal Ministry for Research and Technology (BMFT), the Volkswagen Foundation, and the Deutsche Forschungsgemeinschaft
[n] supported by the Spanish Ministry of Education and Science through funds provided by CICYT
[o] supported by the Particle Physics and Astronomy Research Council
[p] supported by the US Department of Energy
[q] supported by the US National Science Foundation

1 Introduction

Deep-inelastic neutral current scattering is described by the exchange of a virtual boson (γ^*, Z^0) between the electron and a parton in the proton. In the naïve Quark-Parton-Model (QPM), this process leads to a 1+1 parton configuration in the final state which consists of the struck quark and the proton remnant, denoted by "+1". Higher-order QCD processes contribute significantly to the ep cross section at HERA energies: to $\mathcal{O}(\alpha_s)$ these are QCD-Compton scattering (QCDC), where a gluon is radiated by the scattered quark and Boson-Gluon-Fusion (BGF), where the virtual boson and a gluon fuse to form a quark-antiquark pair. Both processes have 2+1 partons in the final state, as shown in Fig. 1.

Jet production in Deep-Inelastic Scattering (DIS) has been studied by a fixed target experiment (E665) at a centre of mass energy, $\sqrt{s}$, of 31 GeV and at negative squared momentum transfers, Q^2, of order 10 GeV^2 [1]. At the much larger centre of mass energy of 296 GeV at HERA, jet structures are much more visible [2, 3]. It is therefore possible in this energy regime to determine the Q^2 dependence of the strong coupling constant, α_s, in a single experiment by measuring the rate of two-jet[1] production [4].

Such measurements require a detailed understanding of jet properties. In this paper we study whether the two-jet system has large enough invariant mass and whether the jets have sufficiently large transverse momenta for perturbative calculations to be applicable. Using Monte Carlo simulations of parton showering and hadronisation to correct for higher-order and non-perturbative effects, the underlying parton dynamics and the jet rates are compared to next-to-leading order (NLO) calculations.

We study jet production in the kinematic range $160 < Q^2 < 1280$ GeV^2, $0.01 < x < 0.1$ and $0.04 < y < 0.95$, at an average squared hadronic invariant mass $\langle W^2 \rangle$ of 14000 GeV^2, where x is the "Bjorken x" variable and y denotes the energy fraction transferred from the incoming electron to the proton in its rest system. The choice of this kinematic range was based on the following expectations: at high Q^2, jet structures should be more pronounced and hadronisation uncertainties should be reduced. Furthermore, in the region $x > 0.01$, the phase space for jet production increases. Also, at $x > 0.01$, the theoretical uncertainties in the jet rates due to different parameterisations for the parton densities of the proton are small [5].

The data were collected with the ZEUS detector in 1993 and correspond to an integrated luminosity of 0.55 pb^{-1}. A brief description of the ZEUS detector is given in section 2. The event selection is explained in section 3. In section 4 we describe the Monte Carlo simulation and the theoretical calculations. The JADE algorithm [6] which is used to relate parton- and hadron-level jets in this paper is described in section 5. The kinematic variables for two-jet production are defined in section 6. In section 7 we study the hadronic energy flows, the pseudorapidity distribution of the jets in the detector, the partonic scaling variables and the jet production rates. Conclusions are given in section 8.

2 The ZEUS detector

The experiment was performed at the electron-proton collider HERA using the ZEUS detector. During 1993 HERA operated with bunches of electrons of energy $E_e = 26.7$ GeV colliding with bunches of protons of energy $E_p = 820$ GeV, with a time between bunch crossings of 96 ns.

[1] In this paper we refer to 2+1 jet production as two-jet production.

ZEUS is a hermetic multipurpose magnetic detector that has been described elsewhere [7, 8]. Only components relevant to this analysis are mentioned here.

The hadronic final state and the scattered electron are measured by the uranium-scintillator calorimeter (CAL). It consists of three parts, the Forward (FCAL), the Rear (RCAL) and the Barrel Calorimeter (BCAL)[2]. Each part is subdivided longitudinally into one electromagnetic section (EMC) and one hadronic section (HAC) for the RCAL or two HAC sections for BCAL and FCAL. Holes of 20×20 cm^2 at the centre of FCAL and RCAL accommodate the HERA beam pipe. In the XY plane around the FCAL beam pipe, the HAC section is segmented in 20×20 cm^2 cells and the EMC section in 5×20 cm^2 cells. In total, the calorimeter consists of approximately 6000 cells. In terms of pseudorapidity $\eta = -\ln\tan\frac{\theta}{2}$, the FCAL covers $4.3 \geq \eta \geq 1.1$, the BCAL $1.1 \geq \eta \geq -0.75$ and the RCAL $-0.75 \geq \eta \geq -3.8$, assuming the nominal interaction point (IP) at $X = Y = Z = 0$. The CAL energy resolution as measured under test beam conditions is $\sigma_E/E = 0.18/\sqrt{E}$ (E in GeV) for electrons and $\sigma_E/E = 0.35/\sqrt{E}$ for hadrons. The timing resolution of the calorimeter is less than 1 ns for energy deposits greater than 4.5 GeV.

The beam monitor scintillation counter (C5) was used to measure the timing of the proton and electron bunches. The event vertices were determined by drift chambers surrounding the beam pipe: the Vertex Detector (VXD) and the Central Tracking Detector (CTD). The resolution of the Z coordinate of the primary vertex is 4 mm.

3 Event selection

3.1 General selection

During the 1993 data-taking period about 10^6 events from the DIS trigger branch were recorded. A more detailed description of the DIS trigger conditions and some aspects of the event selection can be found in [9]. The trigger acceptance was essentially independent of the DIS hadronic final state with an acceptance greater than 97 % for $Q^2 > 10$ GeV^2. In order to select DIS events, the following set of cuts was applied:

- A timing cut required that the event times measured by the FCAL and the RCAL were consistent with an interaction inside the detector. This cut strongly reduced beam-gas background.
- A scattered electron candidate had to be reconstructed with an energy $E_{e'}$ greater than 10 GeV to ensure high purity of the electron sample.
- The position (X, Y) of the scattered electron in the RCAL had to lie outside a square of 32×32 cm^2 centred on the beam axis, to ensure the electron was fully contained within the detector and its position could be reconstructed with sufficient accuracy.

[2] The ZEUS coordinate system is defined as right handed with the Z axis pointing in the proton beam direction, hereafter referred to as "forward". The X axis points towards the centre of HERA, the Y axis points upward. The polar angle θ is taken with respect to the Z direction.

- Events were selected by the requirement $35 < \delta = \sum_i E_i(1-\cos\theta_i) < 60$ GeV, where E_i, θ_i are the energy and polar angle (with respect to the nominal IP) of the calorimeter cells i. For fully contained events $\delta \simeq 2E_e = 53.4$ GeV, where E_e is the electron beam energy. This cut was applied in order to remove background due to photoproduction and beam-gas interactions.

- The Z position of the event vertex was reconstructed from the tracking data. Events were accepted if the Z position was inside ± 75 cm of the nominal IP.

- Events from beam halo muons, cosmic rays and QED Compton processes were identified and rejected by suitable algorithms.

3.2 Kinematics

Because the ZEUS detector is almost hermetic, the kinematic variables x, y and Q^2 can be reconstructed in a variety of ways using combinations of electron and hadronic system energies and angles [10]:

1. The electron method in which the kinematic variables are reconstructed from the energy $E_{e'}$ and angle $\theta_{e'}$ of the scattered electron.

2. The Double Angle (DA) method in which the angles of the scattered electron ($\theta_{e'}$) and of the hadronic system (γ_H) are used. This method reduces the sensitivity to energy scale uncertainties. The angle γ_H corresponds to that of a massless object balancing the momentum vector of the electron to satisfy four-momentum conservation. In the naïve QPM γ_H is the scattering angle of the struck quark. It is determined from the hadronic energy flow measured in the detector using the equation

$$\cos\gamma_H = \frac{(\sum_h p_{\rm X})^2 + (\sum_h p_{\rm Y})^2 - (\sum_h (E - p_{\rm Z}))^2}{(\sum_h p_{\rm X})^2 + (\sum_h p_{\rm Y})^2 + (\sum_h (E - p_{\rm Z}))^2} \qquad (1)$$

   where the sums, $\sum_h$, run over all calorimeter cells h which are not assigned to the scattered electron, and $(p_{\rm X}, p_{\rm Y}, p_{\rm Z})$ is the momentum vector assigned to each cell of energy E. The cell angles are calculated from the geometric centre of the cell and the vertex position of the event.

3. The Jacquet-Blondel (JB) method [11] in which the kinematic variables are calculated from the reconstructed hadronic final state using the momentum vector $(p_{\rm X}, p_{\rm Y}, p_{\rm Z})$ constructed from the energies E and angles θ of the calorimeter cells which are not assigned to the scattered electron.

The electron method gives better resolution in x at low Q^2 while the DA method is less sensitive to the calorimeter energy scale and gives the better mean resolution over the whole x–Q^2 plane. The JB method is used to calculate the visible hadronic energy in the events which will be used in the jet definition. Complete formulae for calculating the variables x, y and Q^2 are to be found in [10]. When it is necessary to distinguish which method has been used the subscripts 'e', 'DA' or 'JB' will be used on the variable concerned.

The data sample used for this analysis had to satisfy the following cuts:

- In the *DA* method, in order that the hadronic system be well measured, it is necessary to require a minimum of hadronic activity in the CAL away from the beampipe. For this purpose the value of $y_{\rm JB} = \sum_h E(1-\cos\theta)/2E_e$ had to be greater than 0.04.
- The value of $y_e = 1 - \frac{E_{e'}}{2E_e}(1-\cos\theta_{e'})$ had to be less than 0.95. This cut rejects photoproduction background.

The kinematic variables Q^2 and x were determined with the *DA* method. Starting from 28200 events with $Q^2_{\rm DA} > 10$ GeV^2, 1020 events remain after selecting the kinematic region $160 < Q^2_{\rm DA} < 1280$ GeV^2 and $0.01 < x_{\rm DA} < 0.1$ for this analysis. The remaining photoproduction background in this high (x, Q^2) data sample is $\lesssim$1%.

The corrected distributions are corrected for detector and acceptance effects and given in the kinematic ranges $160 < Q^2 < 1280$ GeV^2, $0.01 < x < 0.1$ and $0.04 < y < 0.95$. To investigate the evolution of jet structures with Q^2, a low (x, Q^2) data sample of 4230 events is used with $10 < Q^2 < 20$ GeV^2, $0.0012 < x < 0.0024$ and $0.04 < y < 0.95$.

4 QCD calculation and event simulation

4.1 LO simulations

The detector effects were simulated using events generated with the LEPTO 6.1 Monte Carlo program [12] based on the electroweak scattering cross section. We have studied the process $ep \to e'X$ considering γ^* and Z^0 exchange.

The leading order (LO) matrix elements (ME) are used to simulate the QPM process, $\gamma^*+q \to q$, the QCDC process, $\gamma^* + q \to q + g$, and the BGF process, $\gamma^* + g \to q + \bar{q}$ (Fig. 1). In order to obtain finite cross sections for parton emissions, a minimum invariant mass, $m^2_{ij} = y_{\rm min} W^2$, is required for all pairs of final state partons i and j. Higher order parton emissions, which are calculated in the leading log approximation (LLA) of perturbative QCD, are simulated by the Parton Shower (PS) model. The struck parton can radiate partons either before or after the interaction. The amount and the hardness of the radiation depends on the virtuality (mass) of the partons. In order to simulate the hard emission of partons and the higher-order parton showers, a combined option (MEPS) exists. The value $y_{\rm min} = 0.015$ was used. The parameterisation of the parton distribution functions was the MRSD$'_-$ set [13] which has been shown to describe reasonably the HERA measurements of the proton structure function, F_2 [9].

The event generation included the effects of initial- and final-state photon radiation which were calculated with the program HERACLES 4.4 [14]. The simulation of the detector used a program based on GEANT 3.13 [8, 15].

4.2 NLO calculations

The LEPTO 6.1 Monte Carlo event generator uses the exact $\mathcal{O}(\alpha_s)$ matrix element (ME) and the parton shower (PS) in the leading log approximation. It does not include the NLO matrix element calculation. However, the NLO corrections to the 2+1 jet cross section due to unresolved 3+1 jet events and due to virtual corrections are significant [5]. These corrections are included in the program DISJET of Brodkorb and Mirkes [16] and in a similiar program by Graudenz called PROJET [17].

Both programs calculate cross sections at the partonic level in NLO as a function of x and Q^2. PROJET 3.6, in addition, provides cross sections in terms of the parton variables (see section 6), but it does not contain the NLO corrections to the longitudinal cross section[3]. Only the exchange of a virtual photon (γ^*) is considered in the calculations, however the contribution from Z^0 exchange is small (expected to be less than 2% for Q^2 around 1000 GeV^2 [9]).

5 The jet finding algorithm

A jet finding algorithm is necessary to relate the hadronic final states measured in the detector to hard partonic processes. Results on two-jet production in DIS have been published previously by the ZEUS collaboration based on a cone algorithm using a cone of radius $R = \sqrt{(\Delta\eta)^2 + (\Delta\phi)^2} = 1$ [2]; here the cone variables are the pseudorapidity η and the azimuthal angle ϕ.

In this paper we use the JADE algorithm [6], since it is currently the only algorithm which allows comparison to the NLO calculations. The performance of the JADE algorithm in reconstructing jets has been compared to other algorithms in [18]. The JADE algorithm is a cluster algorithm based on the scaled invariant mass

$$y_{ij}^{\mathrm{JADE}} = \frac{2E_iE_j(1-\cos\theta_{ij})}{W^2}$$

for any two objects i and j assuming that these objects are massless. W^2 is the squared invariant mass of the hadronic final state and θ_{ij} is the angle between the two objects of energies E_i and E_j. The minimum y_{ij} of all possible combinations is found. If the value of this minimum y_{ij} is less than the cut-off parameter y_{cut}, the two objects i and j are merged into a new object by adding their four-momenta and the process is repeated until all $y_{ij} > y_{\mathrm{cut}}$. The surviving objects are called jets.

The JADE algorithm is applied at the parton, hadron and detector levels in the HERA laboratory frame. At the detector level, the calorimeter cell energies and positions serve as inputs to the JADE algorithm. For this analysis, the scale parameter used in the JADE algorithm, W^2, is taken at the detector level from just those calorimeter cells associated with the hadronic system, $W^2_{\mathrm{JB}} = s(1-x_{\mathrm{JB}})y_{\mathrm{JB}}$. By using W_{JB}, the detector acceptance corrections for y_{ij} largely cancel.

We have found that the JADE scheme as it is described here leads to smaller hadronisation corrections than the Lorentz invariant E-scheme [19] which uses the exact invariant mass m_{ij} for massive objects. For this analysis, the JADE scheme is used in the HERA laboratory frame.

[3]These corrections are contained in a newer version (PROJET 4.1.1).

The losses in the forward beam pipe of the ZEUS detector are taken into account by adding a fictitious cluster (called pseudo-particle) in the forward direction to which the missing longitudinal momentum for each event is assigned. The pseudo-particle is treated like any other particle in the JADE clustering scheme. No pseudo-particle procedure is used for the parton and hadron levels of the Monte Carlo generator.

6 Two-jet kinematics

The differential cross section for two-jet production depends on five independent kinematic variables [20], here taken as x, Q^2, x_p, z and ϕ^*. The variable ϕ^* is the azimuth between the outgoing parton plane and the lepton scattering plane in the γ^*-parton centre of mass system (CMS) and the variables x_p, z are Lorentz invariant partonic scaling variables.

The event variable x_p is determined by:

$$x_p = \frac{Q^2}{2p \cdot q} = \frac{x}{\xi} \quad (0 \leq x_p \leq 1),$$

where ξ is the fraction of the proton's (longitudinal) momentum P carried by the incoming parton of momentum p ($p = \xi P$) and q is the momentum of the exchanged virtual boson ($Q^2 \equiv -q^2$). Alternatively, one can write:

$$x_p = \frac{Q^2}{Q^2 + \hat{s}}$$

for massless jets, where $\sqrt{\hat{s}}$ is the invariant mass of the two-jet system. This expression is used to determine x_p experimentally. The range of values of x_p is given by x as the lower limit and is a function of $y_{\rm cut}$ at the upper limit:

$$x = \frac{Q^2}{Q^2 + W^2} \leq x_p \leq \frac{Q^2}{Q^2 + y_{\rm cut} W^2}.$$

The jet scaling variable z is related to the angular distribution of the jets in the γ^*-parton CMS:

$$z = \frac{P \cdot p_{\rm jet}}{P \cdot q} = \frac{1}{2}\left(1 - \cos\theta^*_{\rm jet}\right) \quad (0 \leq z \leq 1),$$

where $\theta^*_{\rm jet}$ is the polar angle of the jet in the γ^*-parton CMS. z is measured from the jet, which is assumed to be massless, and reconstructed in the HERA system:

$$z = \frac{E_{\rm jet}(1 - \cos\theta_{\rm jet})}{\sum_i E_i (1 - \cos\theta_i)}$$

where the sum runs over the two reconstructed (massless) jets. In the JADE algorithm, the total hadronic energy is contained in the 2+1 jet system. Since the remnant jet ('+1') has no transverse momentum, $z_{\rm remnant} = 0$ and therefore $z_1 + z_2 = 1$. The minimum value is determined by the value of $y_{\rm cut}$ and is given by:

$$z_{min} = \frac{(1-x)x_p}{x_p - x} y_{\rm cut} \equiv 1 - z_{max}.$$

In this analysis, we integrate over ϕ^* and study the dependence of the two-jet production on x_p and z. The transverse momentum P_T of the jets with respect to the γ^* direction in the γ^*-parton CMS, can be derived from x_p, z and Q^2:

$$P_T = \sqrt{Q^2 \frac{z}{x_p}(1-x_p)(1-z)}.$$

At the $\mathcal{O}(\alpha_s)$ tree level, the singularities in the two-jet cross section are given by [21]:

$$d\sigma_{2+1}^{\mathrm{BGF}} \propto \frac{[z^2+(1-z^2)][x_p^2+(1-x_p^2)]}{z(1-z)} \text{ and } d\sigma_{2+1}^{\mathrm{QCDC}} \propto \frac{1+x_p^2 z_q^2}{(1-x_p)(1-z_q)},$$

where z_q is labelled specifically for the quark jet in the QCDC process. The x_p singularity in the QCDC process results in small jet-jet invariant masses being preferred. Both processes have a singularity at $z = 0$ or 1: in the BGF process, it is related to the collinear emission of the two quarks and, in the QCDC process, to the collinear or soft emission of the gluon. The kinematic properties of the JADE jets and the relationship to these $\mathcal{O}(\alpha_s)$ singularities are studied in section 7.3.

7 Results

7.1 Transverse energy flow in jets

The jet properties were studied at a fixed y_{cut} of 0.02. This value is chosen as a compromise between the increase of the higher-order corrections at lower y_{cut} values and the loss of statistics at higher y_{cut} values for two-jet events. This choice resulted in 237 events with 2+1 jets from a total number of 1020 events in the high (x, Q^2) region. The distributions in the following sections are normalised to the total number of events, N_{ev}.

The transverse energy (E_T) flows relative to the Z axis in the laboratory frame

$$\frac{1}{N_{ev}}\frac{dE_T}{d(\Delta\eta_i)} \quad \text{and} \quad \frac{1}{N_{ev}}\frac{dE_T}{d(\Delta\phi_i)}$$

were calculated with respect to the jet directions in the laboratory frame by defining

$$\Delta\eta_i = \eta_i - \eta_{\mathrm{jet}} \text{ and } \Delta\phi_i = \phi_i - \phi_{\mathrm{jet}}$$

for every calorimeter cell i of 1+1 jet events (Figs. 2a,b and 3a,b) and separately relative to the axes of the higher and the lower η jets of 2+1 jet events (Figs. 2c–f and 3c–f).

In Fig. 2, the E_T flows are compared in two different kinematic regions at low Q^2 ($10 < Q^2 < 20$ GeV^2, $0.0012 < x < 0.0024$) and at high Q^2 ($160 < Q^2 < 1280$ GeV^2, $0.01 < x < 0.1$). The average E_T flow increases with Q^2 and the jets are more collimated at higher Q^2. From kinematics $\langle E_T \rangle \simeq Q$ for the electron and therefore the same is expected for the balancing 1+1 jet. For the two kinematic regions shown here, this corresponds to approximately a factor 5 increase in $\langle E_T \rangle$. The influence of the proton remnant is visible as a tail at $\Delta\eta > 1$ in the 1+1 jet events (Fig. 2b), whereas the tail in Fig. 2d is mainly assigned to the second jet and not the proton remnant.

Fig. 3 shows the E_T flows for the high (x, Q^2) region compared to two Monte Carlo data sets after the detector simulation, generated with the ME and the MEPS options. The E_T flow in terms of the energy scale and the shape around the jet direction is well described, especially when using the MEPS option. In the ME model, the absence of parton showering results in the E_T flow being more concentrated around the jet direction.

Every cell contributing to the E_T flow is assigned to one of the jets by the JADE algorithm. The E_T flow contribution of the jet defining $\Delta\eta = 0$ or $\Delta\phi = 0$ is shown as the shaded histogram in Fig. 3. The JADE algorithm is observed to typically assign cells to a jet inside the range $|\Delta\eta| \lesssim 1$, however, the algorithm also assigns cells beyond this range for the higher η jet (Fig. 3e-f).

7.2 Properties of two-jet events

The two-jet properties are studied in this section for the high (x, Q^2) region. In Fig. 4, the distribution of the pseudorapidity $\eta_{\rm jet}$ of the two jets is shown. The jets are ordered in η. The higher η jet is usually found very close to the forward beam pipe. About half of the jet axes are reconstructed in cells within 30 cm of the FCAL region near the beam pipe ($\theta \lesssim 8^\circ$). In this forward region, the results depend on the description of the initial state parton shower and of the target fragmentation in the Monte Carlo generator, as well as on the simulation of the response of the calorimeter around the beam pipe.

Fig. 4a shows that the predictions of the $\eta_{\rm jet}$ distribution by the ME and the MEPS models describe the data fairly well except for the very forward angles ($\eta_{\rm jet} > 3.6$) where the predictions are below the data for both models. In the region $3.6 > \eta_{\rm jet} > 2.8$ the data are better described by the MEPS model. Most of the lower η jets are also found at positive pseudorapidities in the BCAL or in the FCAL. The Monte Carlo model predictions for the $\eta_{\rm jet}$ distribution of the lower η jet, which is usually well separated from the beam pipe region, gives in general a good description of the data (Fig. 4b).

The distributions of the differences in azimuthal angle, $\Delta\phi_{\rm jet}$, (Fig. 5a) and pseudorapidity, $\Delta\eta_{\rm jet}$, (Fig. 5b) between the two jets show that the jets found by the clustering scheme of the JADE algorithm are reasonably well separated in η. Since ϕ is calculated in the laboratory frame and the electron acquires more transverse momentum at larger values of Q^2, the two jets are not back-to-back in the laboratory frame for the high (x, Q^2) data. This differs from low-Q^2 jet production, where the jets are typically back-to-back in ϕ. The data are generally well described by the Monte Carlo predictions for $\Delta\eta_{\rm jet}$ and $\Delta\phi_{\rm jet}$.

The invariant mass $\sqrt{\hat{s}}$ of the two jets is shown in Fig. 6a. The average invariant mass $\langle\sqrt{\hat{s}}\rangle$ of the jets is about 23 GeV. The $\sqrt{\hat{s}}$ distribution is reasonably well described by the two models. The P_T of the jets in the γ^*-parton CMS, determined from the expression in section 6, is shown in Fig. 6b. (Only the P_T distribution of one of the two jets is shown, since $|P_T^{(1)}| = |P_T^{(2)}|$.) The average value $\langle P_T \rangle$ is about 7 GeV/c. This is sufficiently large to ensure the validity of a perturbative QCD calculation. At low P_T, however, the data lie above the Monte Carlo prediction.

7.3 Partonic scaling variables

The distribution of z versus x_p for the uncorrected data is presented in Fig. 7. The area defined by the curve specifies the kinematic limit for $y_{\rm cut} = 0.02$ in the JADE algorithm and $0.01 < x < 0.1$. The upper and lower limits on x_p depend on x. The upper limit varies in the range $0.34 < x_p < 0.84$ for $0.01 < x < 0.1$, respectively. The data typically lie close to the z limit, given by $z_{min} \simeq y_{\rm cut} = 1 - z_{max}$, which is close to the singular regions of the cross section discussed in section 6.

The measured x_p distribution for the two-jet events is shown in Fig. 8a at the detector level. The bin size has been chosen to reflect the experimental resolution of around 10% in x_p. In the considered (x, Q^2) region, there exists almost no phase space limitation at the upper end of the x_p distribution, with x_p extending up to approximately 0.8 for the high Q^2 data. This is however sufficiently far from the x_p singularity of the QCDC process discussed in section 6. The average x_p is about 0.5, i. e. $\langle \hat{s} \rangle \simeq \langle Q^2 \rangle$. The x_p distribution is well described by the MEPS and the ME models.

The uncorrected x_p distribution for the low Q^2 data which is shown for comparison shows a very different behaviour. It is peaked at small values of x_p, i. e. $\langle \hat{s} \rangle > \langle Q^2 \rangle$, due to the $y_{\rm cut}$ requirement. At these lower Q^2 values, the largest scale is therefore $\hat{s}$.

In the uncorrected z distribution in Fig. 8b, only the z distribution for the jet with smaller z is shown, since $z_1 + z_2 = 1$. At the detector level, the distribution is reasonably well described by both the ME and the MEPS model, but a discrepancy exists for $z < 0.1$ which corresponds to jets close to the forward beam pipe.

The corrected x_p and z distributions are compared to the PROJET NLO calculation in Figs. 8c and d. These distributions were corrected for detector and hadronisation effects with the MEPS simulation. The MRSD$'_-$ parton density parameterisations [13] are used in the calculations of PROJET. Apart from the parameterisation of the parton densities, the QCD calculations contain only one free parameter, the strong coupling constant $\alpha_{\rm s}$. For the calculations in Fig. 8 a value of $\Lambda^{(5)}_{\overline{\rm MS}} = 250$ MeV was chosen which corresponds to $\alpha_{\rm s}(M_Z^2) = 0.120$, as measured from hadronic event shapes, energy correlations and jet rates in $\rm e^+e^-$ annihilations [19].

The shape of the corrected x_p distribution and the PROJET calculation is in good agreement, however, the rate is underestimated. The corrected z distribution is well-described by the calculation for $z > 0.1$, however, an excess is observed in data relative to the PROJET calculation in the lowest z bin. This is, however, the region with the largest systematic uncertainties. The significance of this deviation cannot currently be estimated due to the experimental and theoretical problems associated with the jets in the forward region. The z distributions are almost identical for the ME(LO), not shown, and the PROJET(NLO) calculation. The cross section rises as $z \to 0$, because of the low cut-off with respect to the z singularity in the JADE algorithm.

It should be noted that the jets at the MEPS parton level acquire mass in the JADE algorithm through multiple combinations of partons from the parton shower (PS) whereas the PROJET and the ME jets are defined by massless partons. This effect shifts both the x_p and the z distribution as defined in MEPS, if x_p and z are not calculated in the approximation of massless parton jets.

It should also be noted that the kinematic cut-offs in terms of the partonic scaling variables strongly depend on the choice of jet algorithm. In comparison to the JADE algorithm the $K_\perp$ algorithm [22] leads to a much less peaked z distribution. The $K_\perp$ algorithm was not used for this analysis, because the NLO calculations for DIS are based only on the JADE scheme.

7.4 Jet rates

The two-jet rate R_{2+1} is defined by the ratio

$$R_{2+1} = \frac{N_{2+1}}{N_{2+1} + N_{1+1}},$$

where N_{2+1} and N_{1+1} are the number of 2+1 or 1+1 jet events and $R_{1+1} \equiv 1 - R_{2+1}$. This definition differs from the "usual" definition where the denominator is the total cross section including 3+1 and higher-order contributions. It is used to reduce the dependence on the 3+1 jet rate, which is only calculated at the tree level in PROJET and DISJET. Experimentally, the acceptance correction factors for the 3+1 jet rate are large. For $y_{\rm cut} = 0.02$ about 4% of all events have 3+1 reconstructed jets. Almost no events with 0+1 jets are found in this high (x, Q^2) interval whereas they are often found in the lower (x, Q^2) intervals.

In Fig. 9, the corrected jet production rates are shown as a function of the jet resolution parameter $y_{\rm cut}$. The correction to the parton level is done using the MEPS model. The 2+1 jet rate increases with finer jet resolution (smaller $y_{\rm cut}$). The measured jet rates have been corrected using a bin-by-bin correction method, where the correction factors are up to 20% depending on $y_{\rm cut}$. At lower $y_{\rm cut}$ values ($y_{\rm cut} \simeq 0.02$) the resolution on y_{ij} is approximately 0.01.

For comparison a full NLO calculation performed with the DISJET program and the NLO calculation of the PROJET program are also shown. The difference between the two calculations is attributed to the missing NLO corrections to the longitudinal cross section in PROJET 3.6. The PROJET and DISJET curves are calculated using $\Lambda^{(5)}_{\overline{\rm MS}} = 250$ MeV and the MRSD$'_-$ parton density parameterisations, as discussed in section 7.3. Choosing other currently available parameterisations [23] leads to a variation of the theoretical curves which is of the same order as the statistical errors on the data. The errors shown are the purely statistical binomial errors which are highly correlated, because all 2+1 jet events at a given $y_{\rm cut}$ are included in the points at smaller $y_{\rm cut}$. The data agree with the theoretical calculations at the 15% level, however, a deviation from the QCD models at $y_{\rm cut}$ values below 0.04 is evident in Fig. 9. This deviation is correlated with the excess for $z < 0.1$ discussed in section 7.3.

8 Conclusions

The production of 2+1 jet events as defined by the JADE algorithm has been studied in deep-inelastic neutral current events at HERA for $160 < Q^2 < 1280$ GeV^2, $0.01 < x < 0.1$ and $0.04 < y < 0.95$. In this kinematic range, prominent jet structures have been observed. The transverse energy flows with respect to the jet direction are well described by the LEPTO 6.1 Monte Carlo program. Various measurements of the kinematic properties of the jets have been analysed. They are generally well described by the Monte Carlo models. The invariant mass

and the transverse momentum of the two jets are large enough to allow a description in terms of perturbative QCD. For the first time in DIS, the partonic scaling variables x_p and z have been reconstructed from the jets and are shown to be well described by NLO calculations for $z > 0.1$. Jet rates, corrected to the parton level, have been measured as a function of $y_{\rm cut}$ and compared to NLO calculations. In addition to the structure function parameterisation, the QCD calculations have one free parameter, $\alpha_{\rm s}$, which was taken from LEP measurements. The sensitivity on the choice of parameterisation is small in this kinematic regime. The dynamics of jet production in DIS are satisfactorily described at the 15% level by the calculations. We have refrained at this stage from extracting $\alpha_{\rm s}$ from our data because of the observed sensitivity at very small values of z and the as yet incomplete understanding of this region.

Acknowledgements

We thank the DESY directorate for their strong support and encouragement, and the HERA machine group for their remarkable achievement in providing colliding ep beams. We also gratefully acknowledge the support of the DESY computing and network services.

We would like to thank T. Brodkorb, D. Graudenz and E. Mirkes for valuable discussions and for providing the NLO calculations.

References

[1] E665 Collab., M. Adams et al., Phys. Rev. Lett. 69 (1992) 1026;
H. Melanson (E665 Collab.), Proceedings of the 28th Rencontre de Moriond, Les Arcs, France, March 20–27, 1993.

[2] ZEUS Collab., M. Derrick et al., Phys. Lett. B306 (1993) 158.

[3] H1 Collab., I. Abt et al., Z. Phys. C61 (1994) 59.

[4] H1 Collab., T. Ahmed et al., DESY 94-220, submitted to Phys. Lett. B.

[5] D. Graudenz, Phys. Lett. B256 (1991) 518.

[6] JADE Collab., W. Bartel et al., Z. Phys. C33 (1986) 23;
JADE Collab., S. Bethke et al., Phys. Lett. B213 (1988) 235.

[7] ZEUS Collab., M. Derrick et al., Phys. Lett. B293 (1992) 465.

[8] The ZEUS Detector, Status Report 1993, DESY 1993.

[9] ZEUS Collab., M. Derrick et al., DESY 94-143, accepted for publication in Z. Phys. C.

[10] S. Bentvelsen, J. Engelen and P. Kooijman, Proceedings of the 1991 Workshop on Physics at HERA, DESY Vol. 1 (1992) 23.

[11] F. Jacquet and A. Blondel, Proceedings of the study for an *ep* facility for Europe, DESY 79/48 (1979) 391.

[12] G. Ingelman, Proceedings of the 1991 Workshop on Physics at HERA, DESY Vol. 3 (1992) 1366;
M. Bengtsson, G. Ingelman and T. Sjöstrand, Nucl. Phys. B301 (1988) 554.

[13] A.D. Martin, W.J. Stirling and R.G. Roberts, Phys. Lett. B306 (1993) 145.

[14] A. Kwiatkowski, H. Spiesberger and H.-J. Möhring, Proceedings of the 1991 Workshop on Physics at HERA, DESY Vol. 3 (1992) 1294.

[15] R. Brun et al., CERN DD/EE/84–1 (1986).

[16] T. Brodkorb and E. Mirkes, University of Wisconsin Preprint, MAD-PH-821 (1994).

[17] D. Graudenz, PROJET 3.6, unpublished.

[18] V. Hedberg et al., Z. Phys. C63 (1994) 49.

[19] S. Bethke, Lectures given at the Scottish Universities Summer School, St. Andrews, Scotland, August 1–21, 1993, Heidelberg preprint HD-PY 93/7.

[20] K.H. Streng, T.F. Walsh and P.M. Zerwas, Z. Phys. C2 (1979) 237.

[21] J.G. Körner, E. Mirkes and G.A. Schuler, Int. J. Mod. Phys. A4 (1989) 1781.

[22] B.R. Webber, J. Phys. G19 (1993) 1567.

[23] M. Glück, E. Reya and A. Vogt, Phys. Lett. B306 (1993) 391;
CTEQ Collab., J. Botts et al., Phys. Lett. B304 (1993) 159.

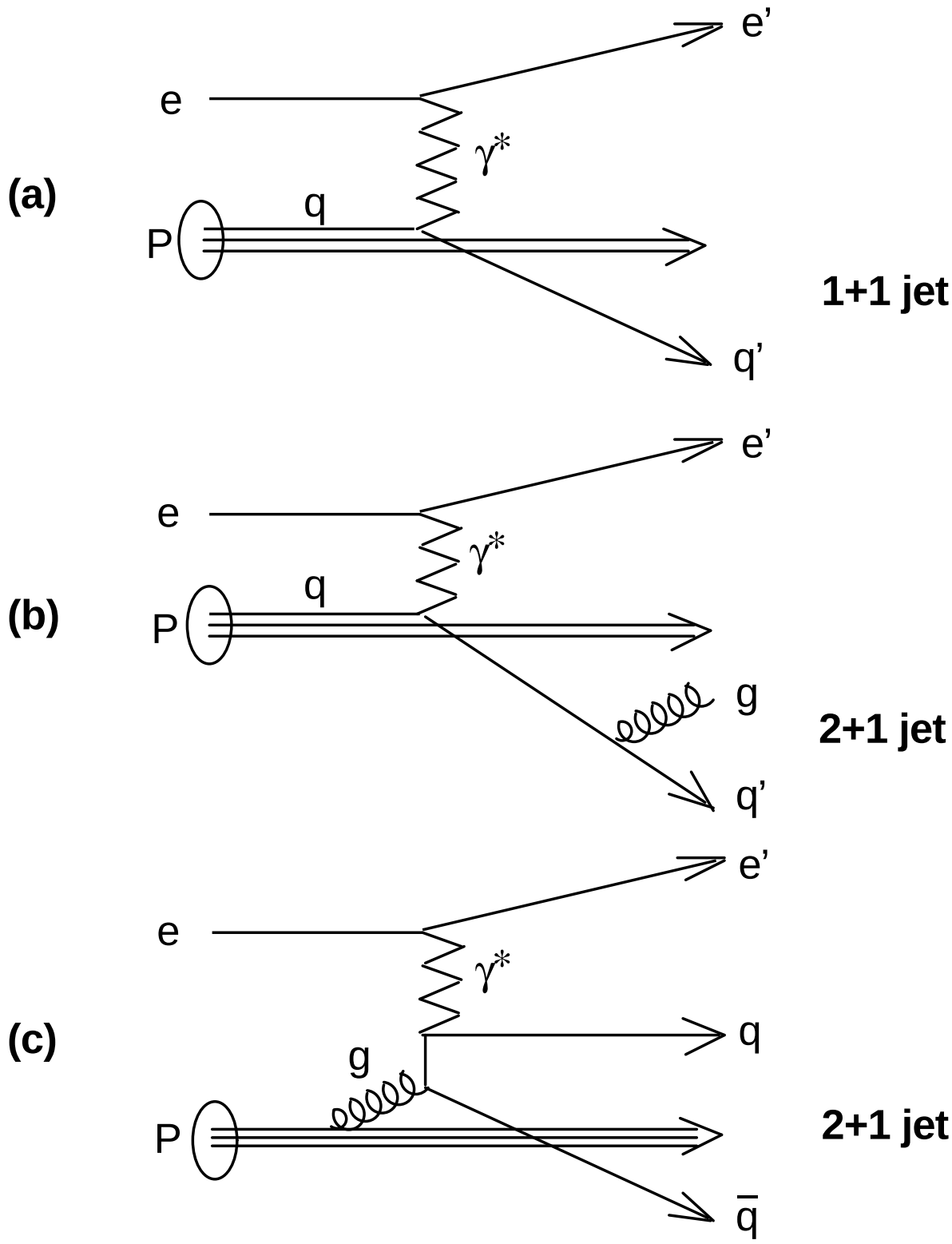

Figure 1: Diagrams for neutral current deep-inelastic scattering: **(a)** Born term, **(b)** QCD Compton scattering, **(c)** Boson-Gluon-Fusion leading to events with 1+1, 2+1 and 2+1 jets, vrespectively.

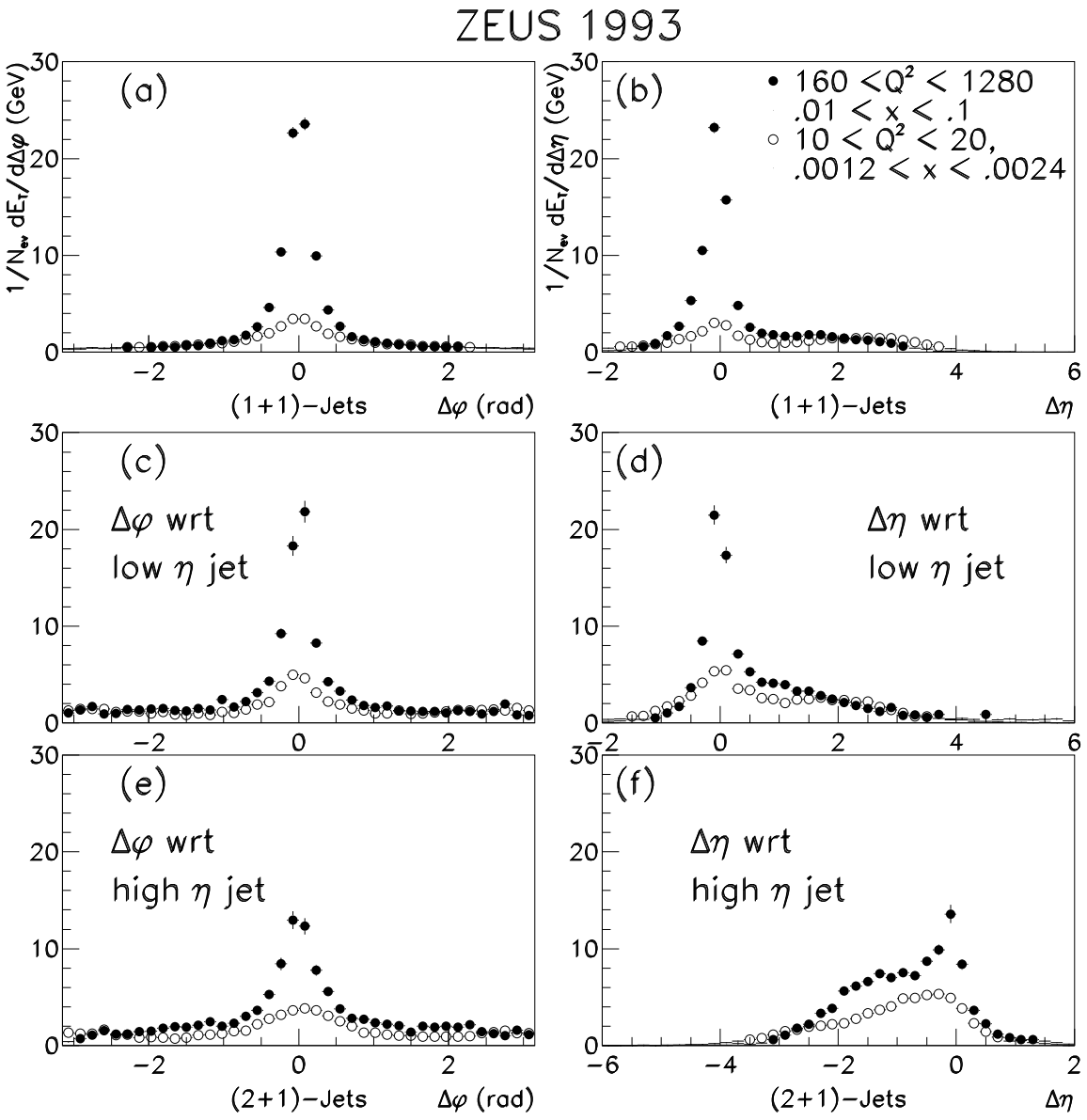

Figure 2: Transverse energy flows in the HERA frame measured relative to the jet directions in 1+1 **(a–b)** and 2+1 **(c–f)** jet events for two (x, Q^2) intervals ($10 < Q^2 < 20$ GeV^2, $0.0012 < x < 0.0024$) and ($160 < Q^2 < 1280$ GeV^2, $0.01 < x < 0.1$). The data are uncorrected and are indicated by the full and open dots, respectively.

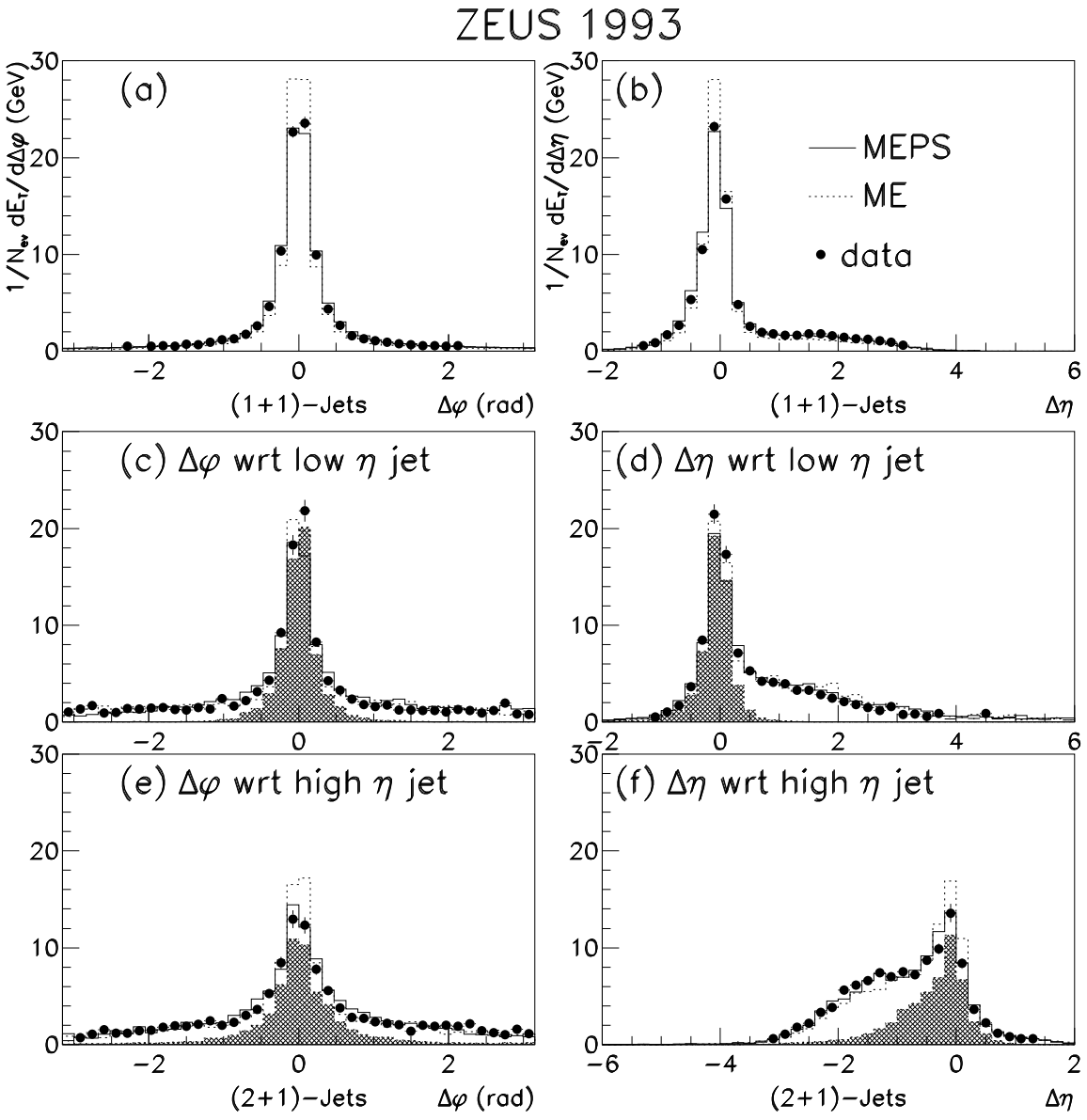

Figure 3: Transverse energy flows in the HERA frame measured relative to the jet directions in 1+1 **(a–b)** and 2+1 **(c–f)** jet events for $160 < Q^2 < 1280$ GeV^2 and $0.01 < x < 0.1$. The data are shown by the full dots. The contribution from the jet which defines $\Delta\eta = 0$ or $\Delta\phi = 0$ for the data is indicated by the shaded histogram. Uncorrected data are compared to the MEPS and the ME simulations.

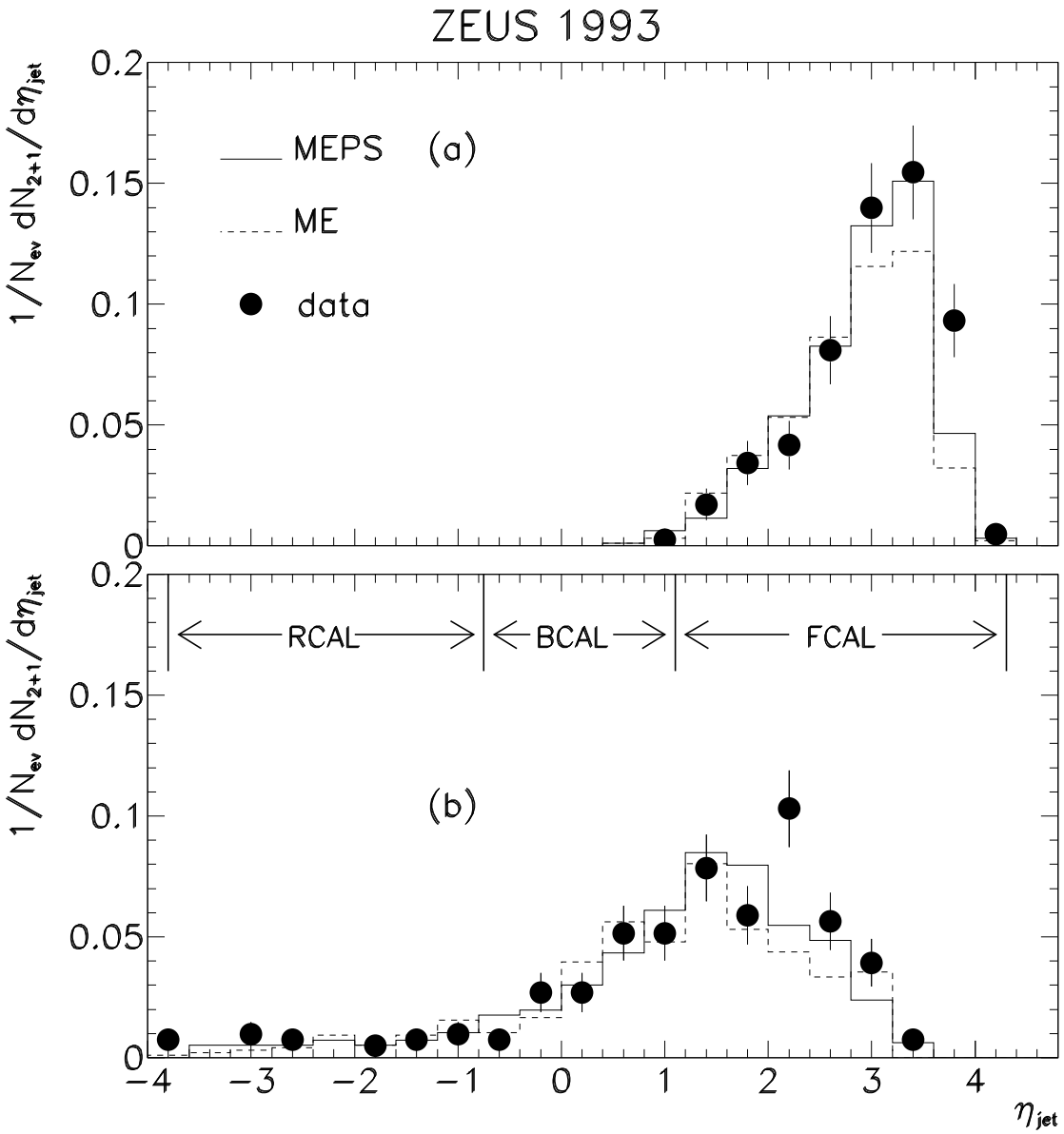

Figure 4: Pseudorapidity $\eta_{\rm jet}$ of the two jets in the kinematic ranges $160 < Q^2 < 1280$ GeV^2, $0.01 < x < 0.1$ and $0.04 < y < 0.95$: **(a)** higher η jet; **(b)** lower η jet. Uncorrected data are compared to the MEPS and the ME simulations. The boundaries of the different calorimeter parts are indicated.

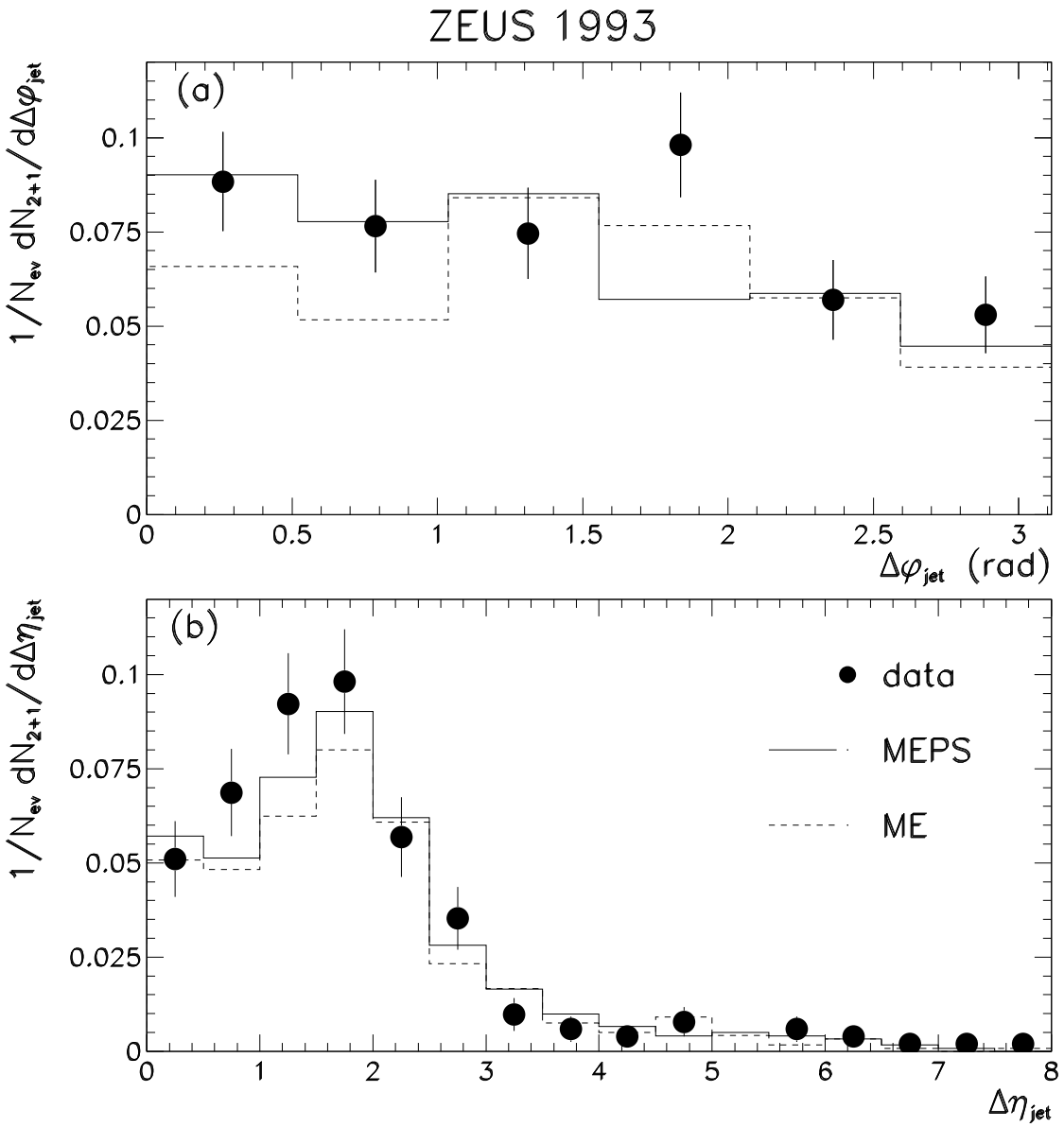

Figure 5: **(a)** The difference in azimuthal angle, $\Delta\phi_{\rm jet}$, and **(b)** pseudorapidity, $\Delta\eta_{\rm jet}$, between the two jets of 2+1 jet events in the kinematic ranges $160 < Q^2 < 1280$ GeV^2, $0.01 < x < 0.1$ and $0.04 < y < 0.95$. Uncorrected data are compared to the MEPS and the ME simulations.

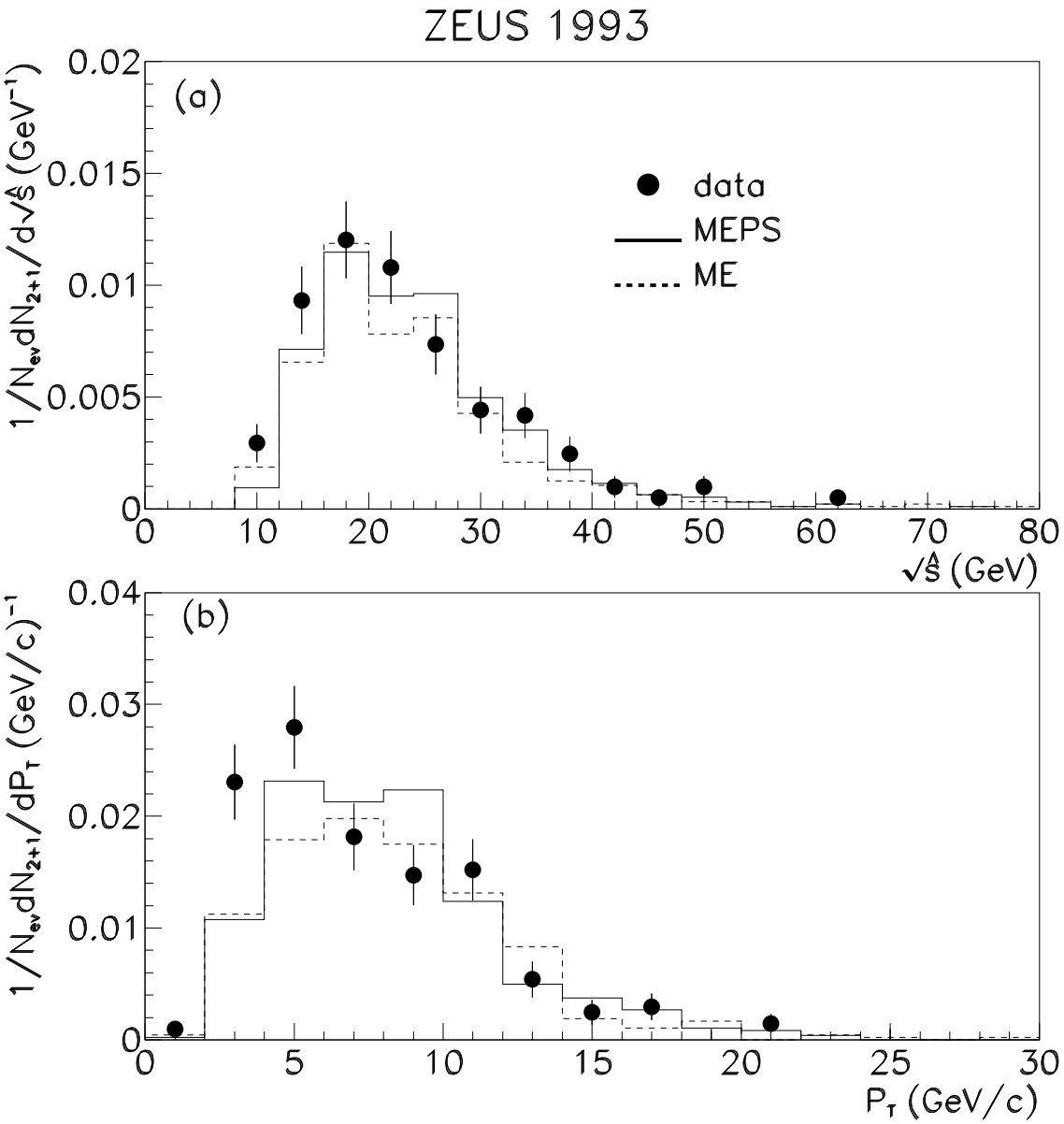

Figure 6: **(a)** The two-jet invariant mass $\sqrt{\hat{s}}$ and **(b)** the jet transverse momentum P_T in the γ^*-parton centre of mass system in the kinematic ranges $160 < Q^2 < 1280$ GeV^2, $0.01 < x < 0.1$ and $0.04 < y < 0.95$. The uncorrected data are compared to the MEPS and the ME simulations.

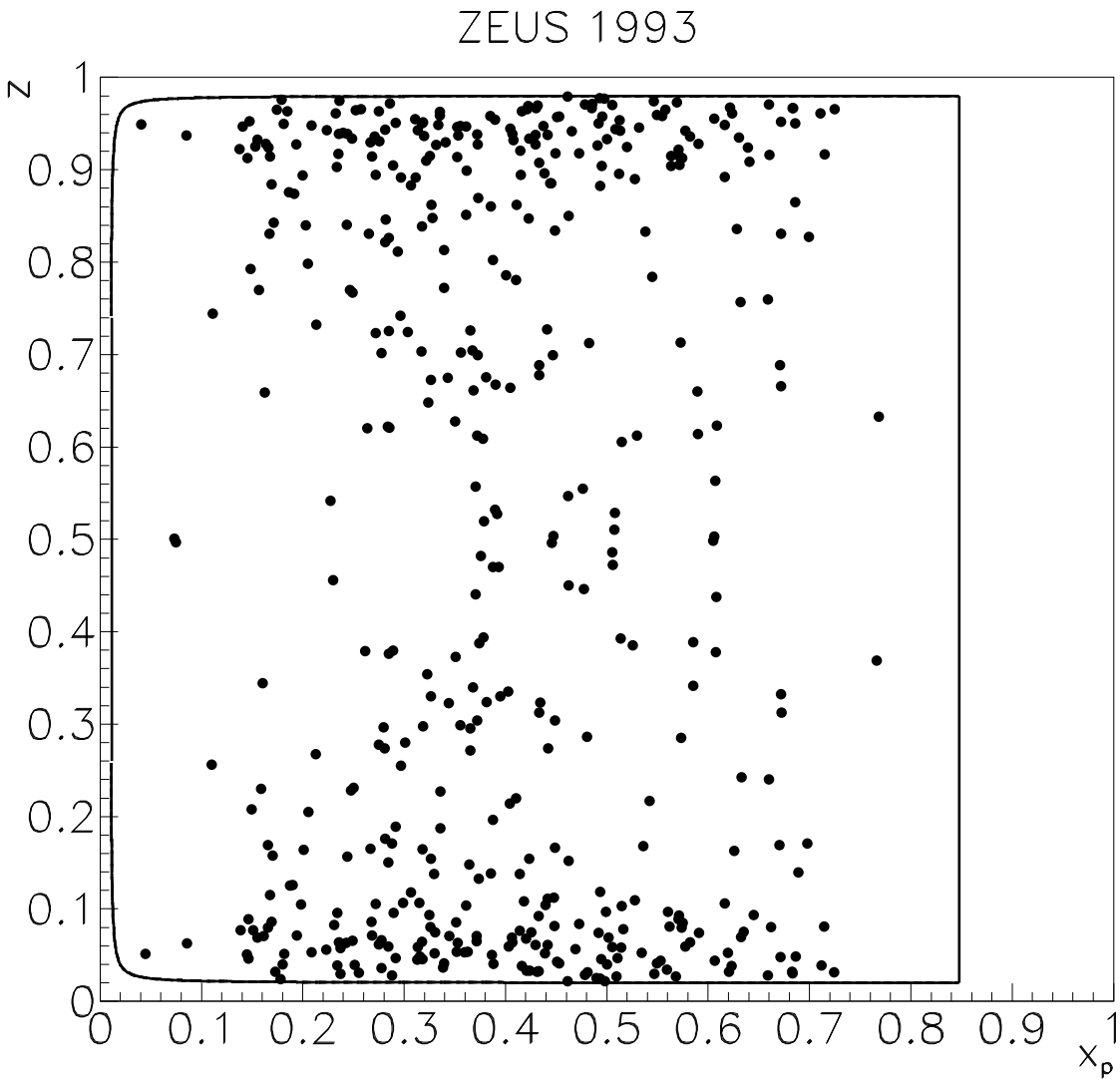

Figure 7: The distribution of z versus x_p for uncorrected data in the high (x, Q^2) interval. The area defined by the curve indicates the kinematic limit for $y_{\rm cut} = 0.02$ in the range $0.01 < x < 0.1$. The limit on z is given by $z_{min} \simeq y_{\rm cut} = 1 - z_{max}$.

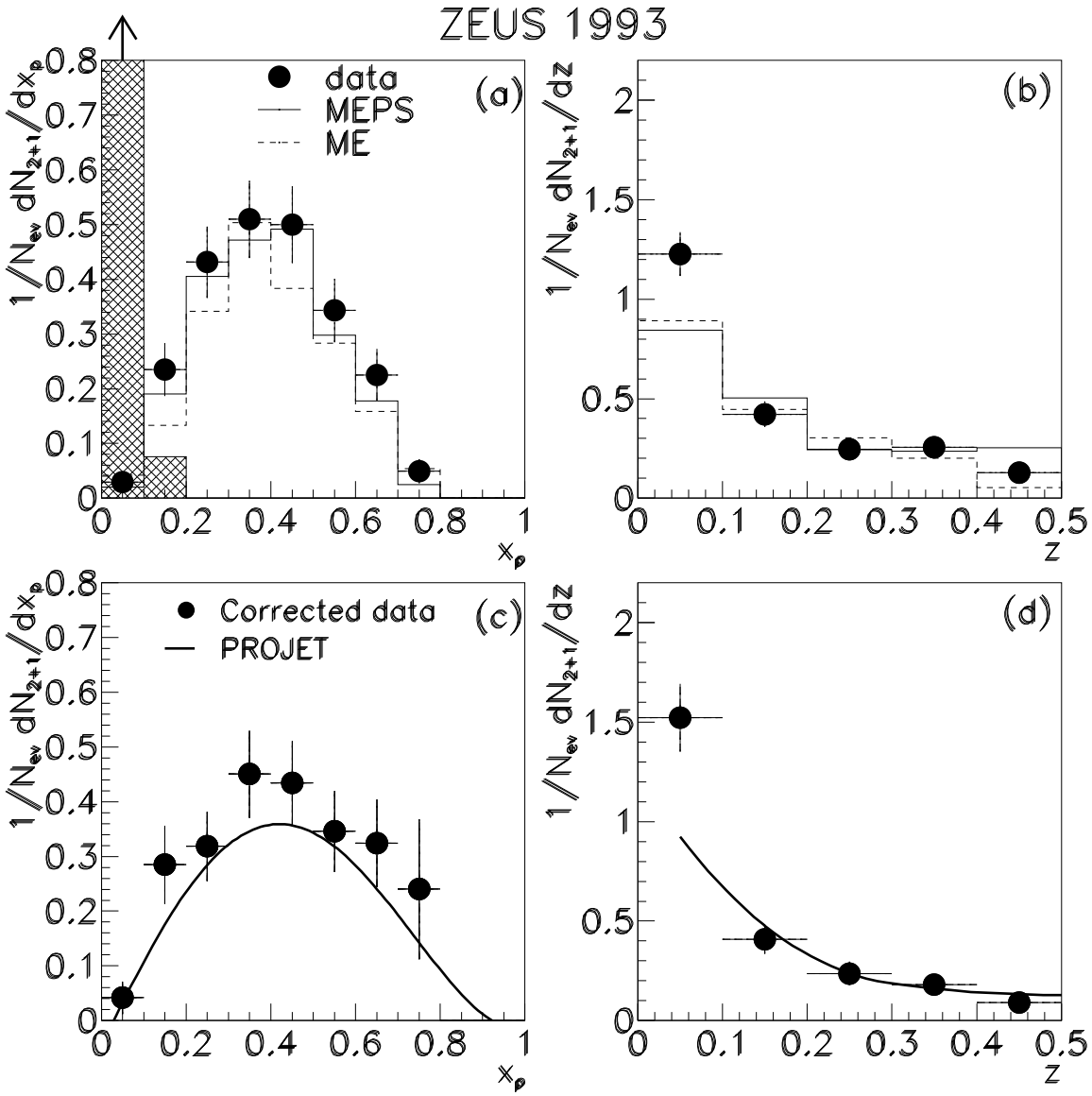

Figure 8: **(a)** Uncorrected x_p distribution of two-jet events and **(b)** uncorrected z distribution of the jet with the smaller z. The uncorrected data are compared to the MEPS and the ME simulations. The shaded histogram in **(a)** shows the uncorrected x_p distribution in the kinematic ranges $10 < Q^2 < 20$ GeV^2, $0.0012 < x < 0.0024$ and $0.04 < y < 0.95$.
(c) corrected x_p distribution and **(d)** corrected z distribution compared to the NLO calculation (PROJET). The data have been corrected with the MEPS simulations. Statistical errors only are shown.

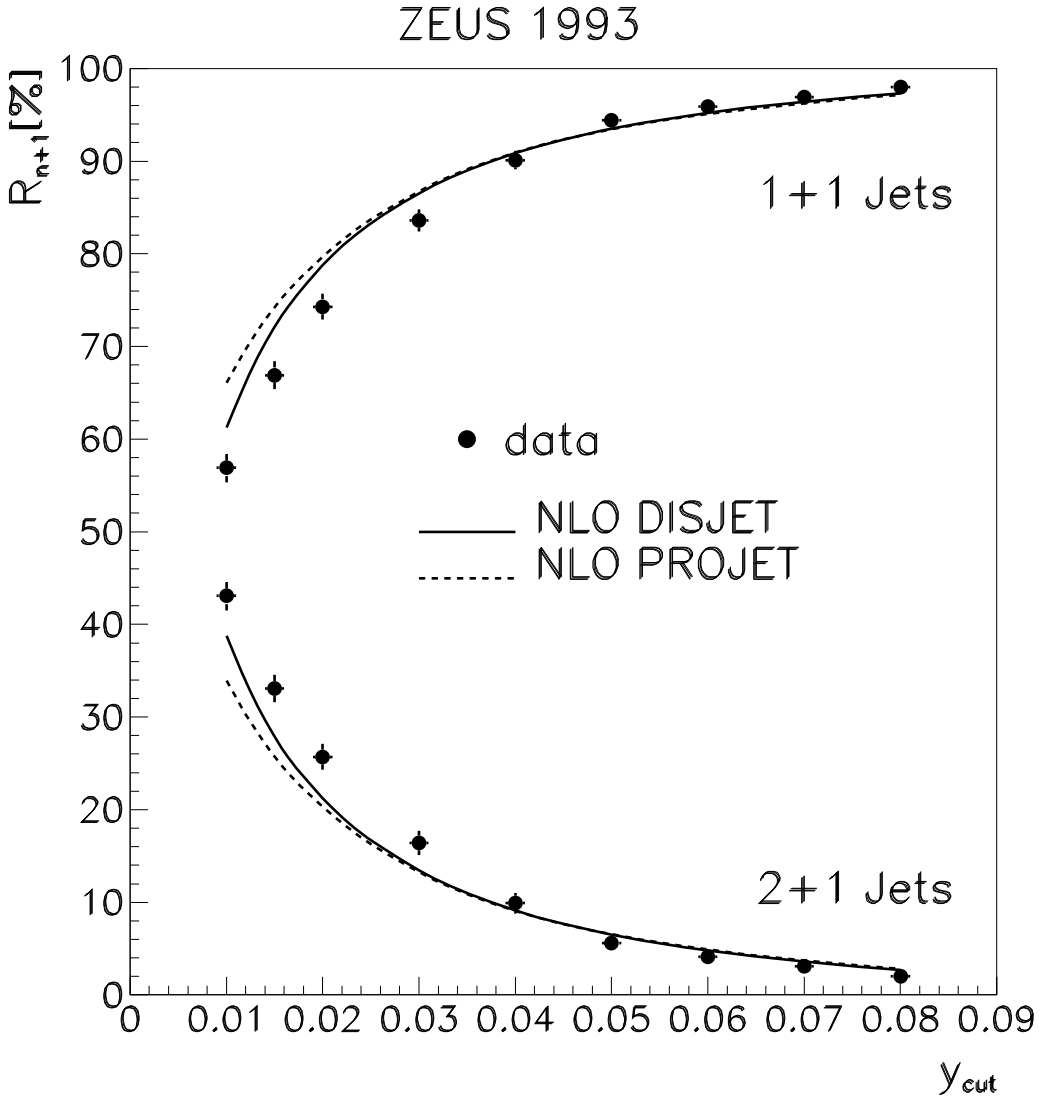

Figure 9: The corrected jet production rate R_{n+1} in % as a function of $y_{\rm cut}$ is compared to the NLO calculation of the programs PROJET [17] and DISJET [16] in the kinematic ranges $160 < Q^2 < 1280$ GeV^2, $0.01 < x < 0.1$ and $0.04 < y < 0.95$. The data have been corrected to the partonic level with the MEPS model. Statistical errors only are shown.